Supporting Information for

The role of point defects in enhancing the conductivity of $BiVO_4$

Hosung Seo[1,2,3*], Yuan Ping[4*] and Giulia Galli[2,3,5†]

1. Department of Physics and Department of Energy Systems Research, Ajou University, Suwon, Gyeonggi 16499, Republic of Korea
2. The Institute for Molecular Engineering, The University of Chicago, Chicago, IL 60615, USA
3. Materials Science Division, Argonne National Laboratory, Argonne, IL 60439, USA
4. Department of Chemistry and Biochemistry, University of California, Santa Cruz, Santa Cruz, CA 95064, USA
5. Department of Chemistry, University of Chicago, Chicago, IL 60615, USA

[*] These authors equally contributed to this work.
[†] Correspondence to gagalli@uchicago.edu

Figure S1. Electronic structure of *n*-doped *ts*-BVO

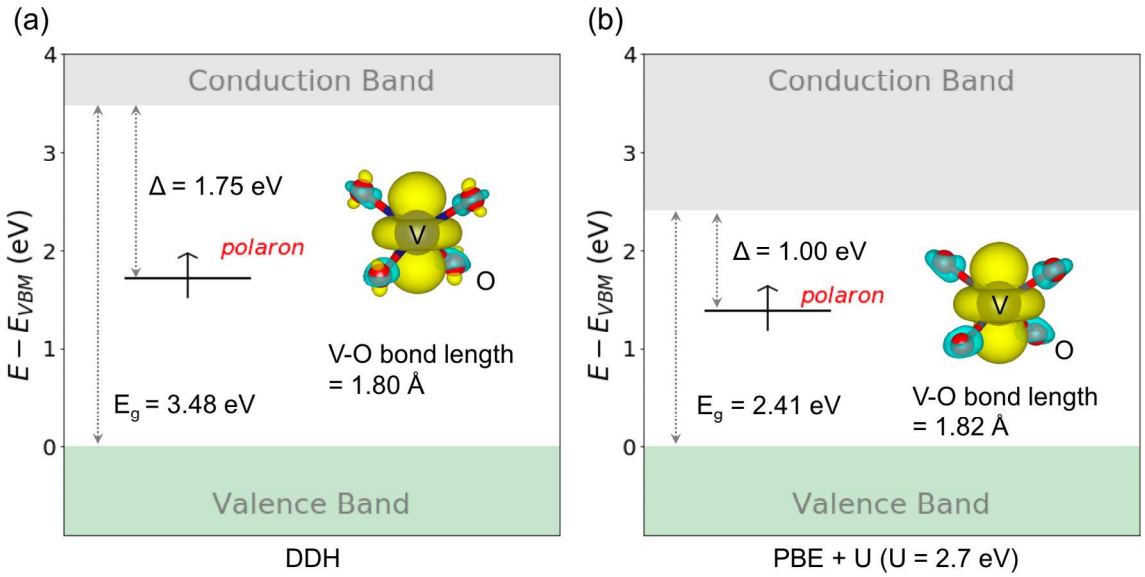

Figure S1. Electronic structure of *ts*-BVO with one extra electron per supercell calculated using the DDH (**a**) and the PBE+*U* (*U*=2.7 eV) functionals (**b**). In both cases, a singly-occupied non-dispersive polaronic state is formed inside the band gap of BVO. Insets show the square modulus of the electronic wavefunction associated with the polaronic state, showing that the excessive electron mainly occupies a V $3d_{z^2}$ orbital. The V^{5+} ion has 4 nearest neighbor O^{2-} ions arranged in a tetrahedral geometry; the crystal field splitting of the V 3*d* manifold yields t_{2g} and e_g states. Additional tetragonal distortions further split the low-lying e_g manifold, pushing the V^{5+} $3d_{z^2}$ orbital lower in energy than the $3d_{x^2-y^2}$ orbital; the latter largely contributes to the character of the CBM[1]. Hence the occupied electronic state localized below the CBM has a V $3d_{z^2}$ character. The ionic relaxation associated with the polaron formation is found to be largely isotropic: the four nearest neighbors O^{2-} ions move outward from the V site by about 0.08 Å at both the DDH and PBE+*U* levels of theory.

Figure S2. Total energy of a BVO crystal with an electron localized at a neutral oxygen vacancy.

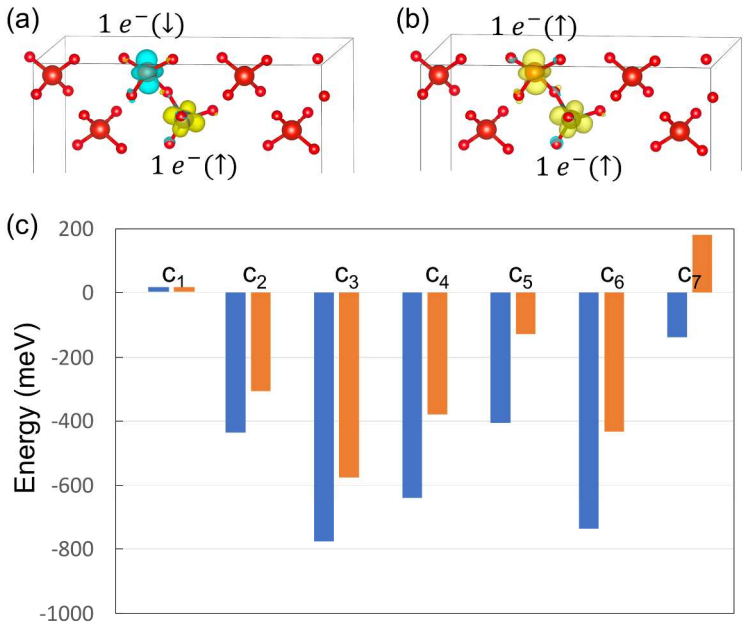

Figure S2. (**a,b**) Singlet (S=0) (**a**) and triplet (S=1) (**b**) spin configurations of two electrons localized at the O vacancy site (configuration c4 in Fig. 3(d)) in $BiVO_4$. In (a) and (b), the spin-up and spin-down densities are shown in yellow and blue, respectively. The energy difference between the two configurations (E(S=1) – E(S=0)) is calculated to be -10.6 meV at the DDH level of theory. The small energy difference implies that the exchange interaction between the two electrons localized at the neutral oxygen vacancy in BVO is negligible and the two spins are independent. (**c**) Total energies of the BVO crystal with an electron localized at a neutral oxygen vacancy (OV), computed using the DDH (blue) and PBE+U (U = 2.7 eV; orange) functionals. The geometrical configurations c1 to c7 are defined in Fig. 2 of the main text; the energy of c1 is chosen as the zero of energy.

Figure S3. Configurations of the OV with a polaron

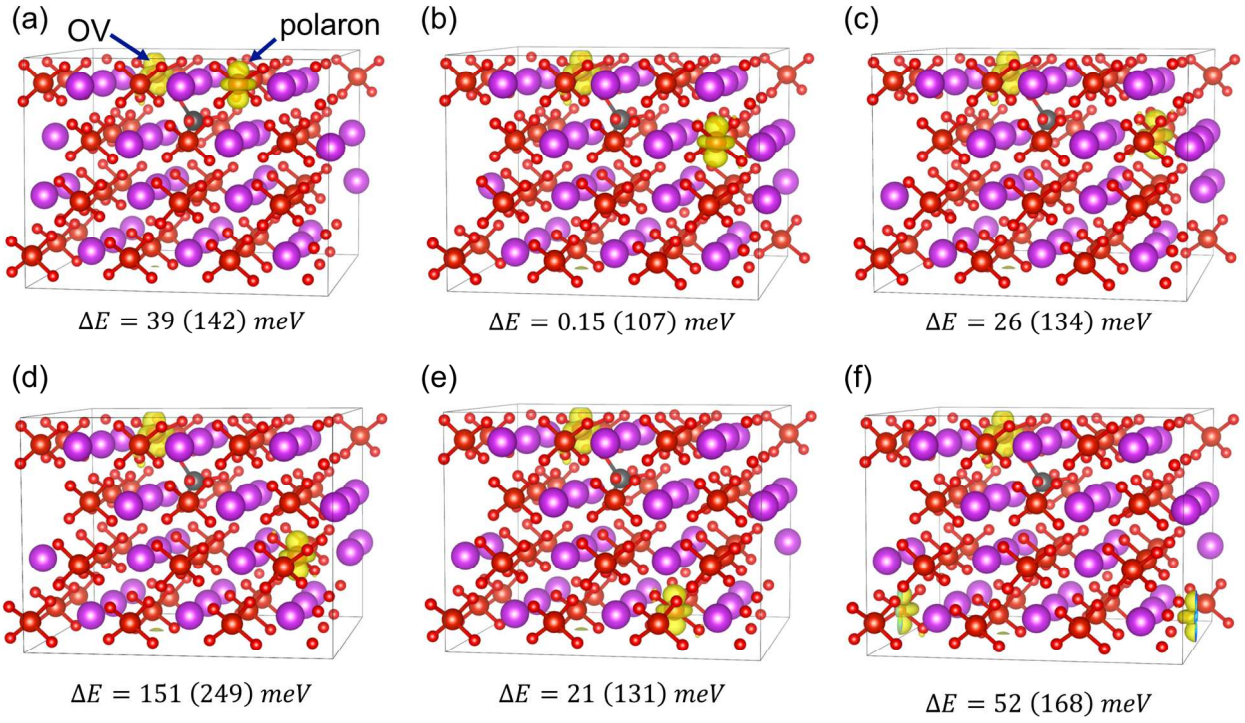

Figure S3. Various configurations of electron polaron in the presence of the O vacancy. The configuration in (a) is the c6 configuration reported in Fig. 3 in the main paper, where one electron forms a small polaron in the bulk region while one electron is trapped at the OV site. The other configurations in (b) to (f) are similar configurations: one electron is trapped at the same OV site and the other electron forms a small polaron at various places in the bulk region of BVO. To calculate the relative energy (ΔE), the energy of the c3 configuration (Fig. 3(c), both of the two electrons are trapped at the OV site) is chosen as the zero of energy.

Figure S4. Configurations of a positively charged oxygen vacancy

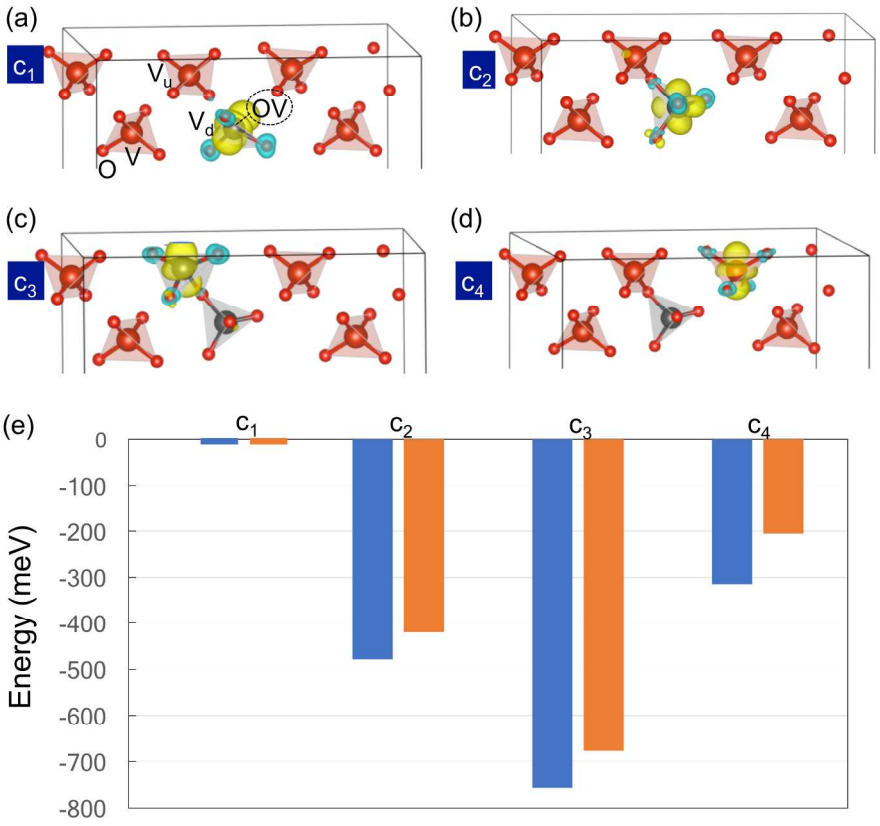

Figure S4. Several configurations of electrons localized near a positively charged oxygen vacancy (OV^+) in BVO (**a** to **d**), and corresponding total energies of the defect states computed using the DDH (blue) and PBE+U (U = 2.7 eV; orange) functionals (**e**). Vanadium and oxygen atoms are represented by large and small red spheres, respectively. Bi atoms and some of VO_4 tetrahedra are omitted for clarity. (**a**) An electron originating from the OV^+ (represented by a dotted sphere) is localized at a V atom site (labeled as V_d and represented by a black sphere) in the O-deficient VO_3 unit. (**b to d**) OV configurations where the O-deficient VO_3 unit has a nearly VO_4 tetrahedral geometry, where one O ion is shared with a nearest neighboring VO_4 unit whose V atom is labeled as V_u. The extra electron donated by the OV^+ can be both trapped at the V_d site (**b**) or at the V_u site (**c**). In (**d**), we show a configuration where the extra electron leaves the OV^+ site and forms a small polaron in the bulk region of BVO. In the diagram reported in (**e**), total energies are refereed to that of the c1 configuration.

Figure S5. Defect formation energies obtained with the PBE+U functional

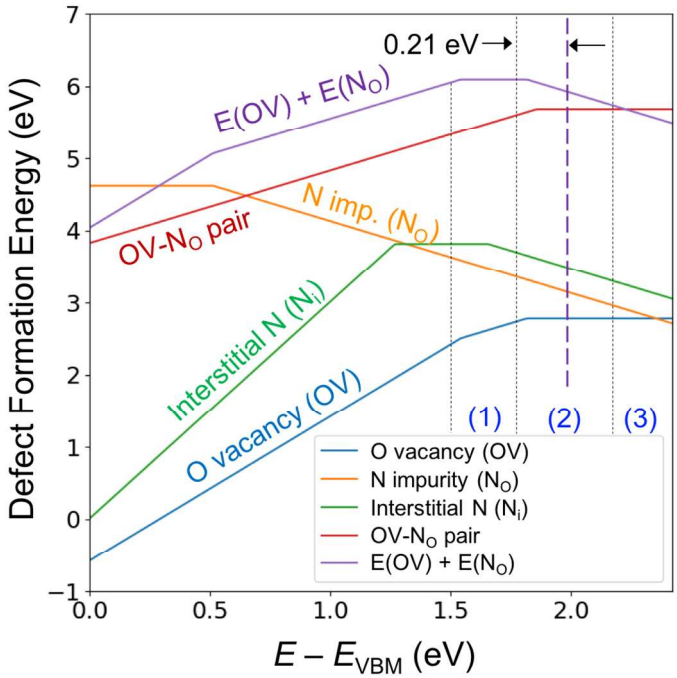

Figure S5. Defect formation energies (DFEs) of an oxygen vacancy (OV), a substitutional nitrogen (N_O), a interstitial nitrogen (N_i) and an OV-N_O pair in BVO in the O-rich limit, calculated by using the PBE+U (U = 2.7 eV) functional. The DFE is calculated as a function of Fermi level (E) from the valence band maximum (VBM, E_{VBM}) to the CBM, which is the right end of the plot. There are three distinctive regions of stability for OV and OV-N_O pairs, near the CBM, denoted as (1), (2), and (3) (see the main text). The figure shows the lowest energy configurations for all defects and all charge states. Some of the meta-stable states (higher in energy) found in our calculations are reported in the SI (e.g. see Fig. S4 for a positively charged OV). The slope of a DFE line corresponds to the charge state of the defect, and the position of the Fermi level where two different charge states intersect yields the charge transition level (CTL, see Eq.1). The energy difference between the (+1/0) CTL of the OV (black, vertical, dotted line dividing the area (1) and (2)) and the CBM defines the ionization energy of the neutral OV with respect to the CBM. The vertical, purple, dashed line indicates the polaron level in BVO and the difference between this line and the (+1/0) CTL of the OV is calculated to be 0.21 eV; this energy corresponds to the ionization energy of the neutral OV with respect to the polaron level in BVO.

Figure S6. Electron localized at a substitutional nitrogen site

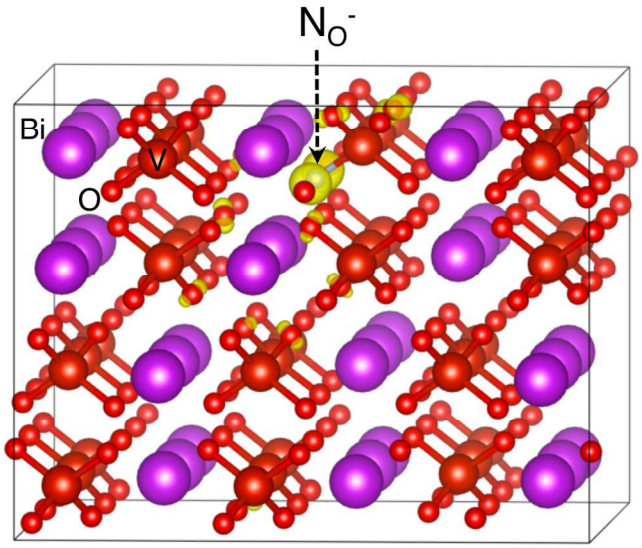

Figure S6. Square modulus of the wavefunction of the highest occupied defect state associated with the presence of a substitutional N dopant. An extra electron added to the supercell is mostly localized at the N site, indicating that N^{3-} configuration is energetically favored. In addition, we found that the occupied N_O-induced band is within 0.2 eV from the VBM (at the DDH level of theory), giving rise to a level resonant with the O 2p states.

Figure S7. Ground-state structure of a neutral oxygen vacancy-nitrogen dopant complex

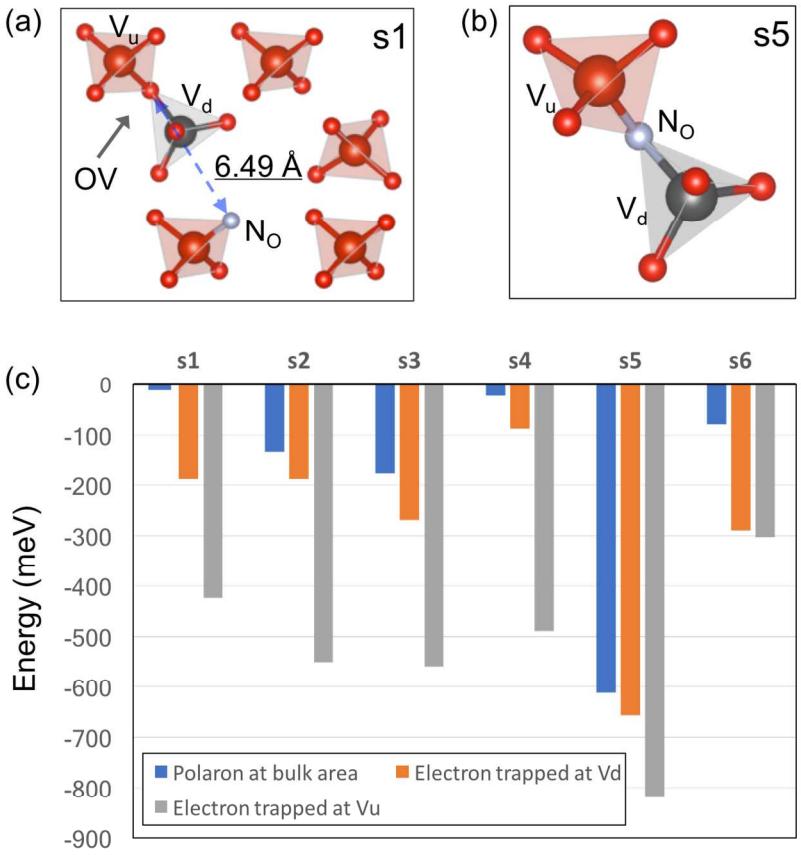

Figure S7. Ground-state structure of a neutral oxygen vacancy-nitrogen dopant (OV-N_O) defect complex (q = 0). In the neutral charge state, two extra electrons are donated by each OV, with one electron tightly bound to the N_O site, as discussed in the main text. The state of the neutral OV-N_O pair is characterized by (1) the distance between the N_O and the OV and (2) the localization site of the extra electron. In **(a)** and **(b)**, the N_O is placed at a distance of 6.49 Å (labeled as s1) and 0 Å (labeled as s5), respectively, from the OV, whose central position is defined to be the joint position of the corner-sharing VO_4 tetrahedra. We also considered cases in which the N_O is placed at different O sites of the corner-sharing VO_4 tetrahedra, which are labeled as s2, s3, s4, and s6. For a given OV-N_O distance, the excess electron can be trapped either at the V_d or the V_u site, or it can form a polaron in the bulk region of BVO away from the OV structure. The graph in (**c**) compares the total energy of different possible configurations of the neutral OV-N_O defect, calculated at the PBE+U level of theory; we found that the s5 configuration is the ground state, with the extra electron trapped at the V_u site, the same as the ground-state structure of the positively charged OV-N_O discussed in Fig. 4.

Table S1. Computed bulk properties of *ts*-$BiVO_4$ at the PBE, PBE+U, and DDH levels of theory. The lattice parameters, several bond lengths, and the band gap are reported. Note that the computed fundamental gap does not include spin-orbit coupling and temperature effects, which are supposed to lower the gap obtained here[2] by ~ 0.15 and 0.5 eV, respectively.

	Lattice parameters (Å)		Bond lengths (Å)		Band gap (eV)
	a	c	V-O	Bi-O	Indirect
PBE, this work	5.174	11.768	1.735	2.462 / 2.506	2.32
PBE+*U*, this work	5.173	11.771	1.740	2.450 / 2.510	2.41
DDH, this work	5.133	11.682	1.722	2.436 / 2.492	3.48
PBE0 hybrid functional[3]	5.121	11.647	1.721	2.431 / 2.481	3.25
Experiment[4-8]	5.147	11.722	1.72	2.453/2.499	2.4-2.5 (optical gap)

Table S2. Relative charge transition levels of the OV, N_O, and OV-N_O defects with respect to the conduction band edge calculated at the DDH and DFT+U levels of theory.

Defect type	CTL type	DDH CTL (eV)	DFT+U CTL (eV)
OV	(+2/+1)	1.15	0.89
	(+1/0)	0.77	0.61
N_O	(0/-1)	2.38	1.92
OV-N_O	(+1/0)	0.83	0.57

Supplementary reference

1. Kweon, K.; Hwang, G.; Kim, J.; Kim, S., Electron small polarons and their transport in bismuth vanadate: a first principles study. *Phys. Chem. Chem. Phys.* **2015,** 17, 256-260.
2. Wiktor, J.; Reshetnyak, I.; Ambrosio, F.; Pasquarello, A., Comprehensive modeling of the band gap and absorption spectrum of BiVO4. *Phys. Rev. Mater.* **2017,** 1, 022401(R).
3. Kweon, K.; Hwang, G., Hybrid density functional study of the structural, bonding, and electronic properties of bismuth vanadate. *Phys. Rev. B* **2012,** 86, 165209.
4. Sleight, A.; Chen, H.; Ferretti, A.; Cox, D., Crystal-growth and structure of BiVO4 *Mater. Res. Bull.* **1979,** 14, 1571-1581.
5. Payne, D.; Robinson, M.; Egdell, R.; Walsh, A.; McNulty, J.; Smith, K.; Piper, L., The nature of electron lone pairs in BiVO4. *Appl. Phys. Lett.* **2011,** 98, 212110.
6. Stoughton, S.; Showak, M.; Mao, Q.; Koirala, P.; Hillsberry, D.; Sallis, S.; Kourkoutis, L.; Nguyen, K.; Piper, L.; Tenne, D.; Podraza, N.; Muller, D.; Adamo, C.; Schlom, D., Adsorption-controlled growth of BiVO4 by molecular-beam epitaxy. *Apl Mater.* **2013,** 1, (4), 042112.
7. Cooper, J.; Gul, S.; Toma, F.; Chen, L.; Glans, P.; Guo, J.; Ager, J.; Yano, J.; Sharp, I., Electronic Structure of Monoclinic BiVO4. *Chem. Mater.* **2014,** 26, 5365-5373.
8. Cooper, J.; Gul, S.; Toma, F.; Chen, L.; Liu, Y.; Guo, J.; Ager, J.; Yano, J.; Sharp, I., Indirect Bandgap and Optical Properties of Monoclinic Bismuth Vanadate. *J. Phys. Chem. C* **2015,** 119, 2969-2974.